Dicopper(II) Chloro and Azido Inclusion Complexes of the [24-ane-N_2S_4] Binucleating Macrocycle. Synthesis, Crystal and Molecular Structures, and Spectral, Magnetic, and Electrochemical Properties

Yvette Agnus,[†] Rémy Louis,[†] Jean-Paul Gisselbrecht,[‡] and Raymond Weiss*[†]

Contribution from the Laboratoire de Cristallochimie et de Chimie Structurale (E.R.A. 008 du C.N.R.S.) and Laboratoire d'Electrochimie et de Chimie Physique du Corps Solide (E.R.A. 468 du C.N.R.S.), Institut Le Bel, Université Louis Pasteur, 67070 Strasbourg Cedex, France. *Received May 2, 1983*

Abstract: The tetrachloro and tetraazido dinuclear Cu(II) complexes $[(CuCl_2)_2(C_{18}H_{38}N_2S_4)]$ (**2**) and $[Cu_2(N_3)_4(C_{18}H_{38}N_2S_4)]$ (**3**) of the polyaza-polythia macrocyclic ligand **1** ([24-ane-N_2S_4], 1,3-diaza-4,10,16,22-tetrathiacyclotetracosane) have been prepared and their crystal structures have been determined. In both cases, the two copper ions are located inside the molecular cavity, but large differences appear in bonding to the NS_2 chelating subunits situated at the two poles of the macrocycle **1**, intermetallic distances, and ligand conformation. Complex **2** crystallizes in the monoclinic space group $P2_1/c$ (a = 7.943 (2) Å, b = 22.481 (6) Å, c = 17.538 (5) Å, β = 100.97 (2)°, Z = 4). In the molecular complex $|(CuCl_2)_2 \subset \mathbf{1}|$ the two $CuCl_2$ units are not equivalent. The two copper cations are pentacoordinate $CuNS_2Cl_2$ centers with square-based pyramidal geometry, involving the NS_2 ligand's donor set and one chlorine in the square base. The Cu···Cu distance is 7.228 (1) Å and the macrocycle is in a boat-type conformation. Complex **3** crystallizes in the monoclinic system, space group $C2/m$ (a = 10.126 (2) Å, b = 13.246 (3) Å, c = 11.156 (2) Å, β = 93.47 (1)°, Z = 2). In the $|N_3Cu(N_3)_2CuN_3 \subset \mathbf{1}|$ unit, the two Cu(II) centers are doubly bridged by two azide ions bound end to end. Each Cu(II) displays an elongated octahedral coordination with four equatorial nitrogens and two axial sulfurs with a long Cu–S distance of 2.919 (1) Å. The two Cu(II) and all nitrogens are located in the symmetry plane. The Cu–Cu distance is 5.145 (1) Å and the macrocycle is in a chair-type conformation. The temperature dependences of the magnetic susceptibilities for **2** and **3** show that in **2** no coupling arises between the Cu(II) ions as expected by the long intermetallic distance and the lack of bridging groups, whereas **3** exhibits a diamagnetic behavior resulting from a very strong antiferromagnetic interaction despite the large intermetallic separation. This interaction is attributed to the very similar energies and favorable relative orientation of the orbitals on the bridging atoms and on the metallic ions. The electron-transfer properties of **2** and **3** in Me_2SO solution have been studied by voltammetry, cyclic voltammetry, and coulometry. The dinuclear Cu(II) complexes both undergo a two-electron reversible reduction into their dinuclear Cu(I) species, occurring via two subsequent monoelectronic transfers at positive potentials +0.20 and +0.10 V vs. SCE respectively for **2** and **3**′ ($[Cu_2(N_3)_2 \subset \mathbf{1}]^{2+}$ or $[Cu_2(N_3)_2(Me_2SO)_2 \subset \mathbf{1}]^{2+}$). These properties are related to the flexibility, the nature of the donor atoms, and the macrocyclic framework of ligand **1**.

We have briefly reported the structures and several physicochemical properties relative to the coordination compounds of the macrocyclic binucleating ligand 1,13-diaza-4,10,16,22-tetrathiacyclotetracosane.[1] The coordination chemistry of binuclear transition-metal complexes has been the subject of extensive investigations relating to the synthesis of model compounds for the metal-binding sites of metallobiomolecules. Several copper enzymes contain a pair of copper atoms that are strongly antiferromagnetically coupled. Such binuclear active sites (type 3) are present in the multicopper oxidases where they are associated with the type 1 or blue copper centers and the type 2 copper atoms.[2] These multicopper enzymes catalyze the oxidation of numerous substrates with the concomitant conversion of molecular oxygen into water by multielectron-transfer processes. Hemocyanin,[2-5] the oxygen carrier in *Mollusca's* and *Anthropoda's* blood, and tyrosinase,[2b,3,6] which involves oxygen in monophenol hydroxylation and in *o*-diphenol dehydrogenation, contain only this type of binuclear entities. All these metalloproteins constitute reversible electrochemical systems that perform multielectronic transfers at largely positive standard potentials,[7] propitious to the stabilization of the copper(I) systems in aqueous media. Chemical and spectroscopic studies[2b,4] and EXAFS data[5] of the biological material have led to a unique delineation for the copper binding sites in hemocyanin and tyrosinase.

In the recent past, several binuclear copper(II) and copper(I) complexes have been characterized and are of direct relevance to model systems for copper proteins.[8] The large magnitude of the magnetic exchange coupling occuring in the binuclear active site has been observed in monobridged[9,10] and in dibridged[1,11] binuclear complexes with azide or oxygen-containing anions as

[†] Laboratoire de Cristallochimie et de Chimie Structurale.
[‡] Laboratoire d'Electrochimie et de Chimie Physique du Corps Solide.

(1) (a) Agnus, Y.; Louis, R.; Weiss, R. *J. Am. Chem. Soc.* **1979**, *101*, 3381-3384. (b) Louis, R.; Agnus, Y.; Weiss, R.; Gisselbrecht, J. P.; Gross, M. *Nouv. J. Chim.* **1981**, *5*, 71-73. (c) Comarmond, J.; Plumeré, P.; Lehn, J. M.; Agnus, Y.; Louis, R.; Weiss, R.; Kahn, O.; Morgenstern-Badarau, I. *J. Am. Chem. Soc.* **1982**, *104*, 6330-6340. (d) Agnus, Y. L. "Copper Coordination Chemistry:Biochemical and Inorganic Perspectives"; Karlin, K. D., Zubieta, J. A., Ed.; Adenine Press: New York, 1983; pp 371-393.

(2) (a) Fee, J. A. *Struct. Bonding (Berlin)* **1975**, *23*, 1-60. Malkin, R.; Malmström, B. G. *Adv. Enzymol. Relat. Areas Mol. Biol.* **1970**, *33*, 177-244. Reinhammar, B. *Adv. Inorg. Biochem.* **1979**, *1*, 91-118. Lubien, C. D.; Winkler, M. E.; Thamann, T. J.; Scott, R. A.; Co, M. S.; Hodgson, K. O.; Solomon, E. I. *J. Am. Chem. Soc.* **1981**, *103*, 7014-7016 and references therein. (b) Solomon, E. I.; Penfield, K. W.; Wilcox, D. E. *Struct. Bonding (Berlin)* **1983**, *53*, 1-57. "Copper Proteins"; Spiro, T. G., Ed.; Wiley-Interscience: New York, 1981.

(3) "Structure and Function of Hemocyanin"; Bannister, J. V., Ed.; Springer-Verlag: West Berlin, 1977. "Invertebrate Oxygen Binding Proteins"; Lamy, J., Ed.; Marcel Dekker: New York, 1981. Beinert, H. *Coord. Chem. Rev.* **1980**, *33*, 55-85.

(4) Freedman, T. B.; Loehr, J. B.; Loehr, T. M. *J. Am. Chem. Soc.* **1976**, *98*, 2809-2815. Larrabee, J. A.; Spiro, T. G. *Ibid.* **1980**, *102*, 4217-4223. Himmelwright, R. S.; Eickman, N. C.; Lubien, C. D.; Solomon, E. I. *Ibid.* **1980**, *102*, 5378-5388.

(5) Brown, J. M; Powers, L.; Kincaid, B.; Larrabee, J. A.; Spiro, T. G. *J. Am. Chem. Soc.* **1980**, *102*, 4210-4216. Co, M. S.; Hodgson, K. O.; Eccles, T. K.; Lontie, R. *Ibid.* **1981**, *103*, 984-986. Co, M. S.; Scott, R. A.; Hodgson, K. O. *Ibid.* **1981**, *103*, 986-988. Co, M. S.; Hodgson, K. O. *Ibid.* **1981**, *103*, 3200-3201.

(6) Himmelwright, R. S.; Eickman, N. C.; Lubien, C. D.; Lerch, K.; Solomon, E. I. *J. Am. Chem. Soc.* **1980**, *102*, 7339-7344 and references therein. Winkler, M. E.; Lerch, K.; Solomon, E. I. *Ibid.* **1981**, *103*, 7001-7003.

(7) Malmström, B. G. *Adv. Chem. Ser.* **1977**, *162*, 173-178.

(8) Ibers, J. A.; Holm, R. H. *Science (Washington DC)* **1980**, *209*, 223-235.

0002-7863/84/1506-0093$01.50/0 © 1984 American Chemical Society

Scheme I. Reaction Sequence for the Synthesis of the Macrocycle 1

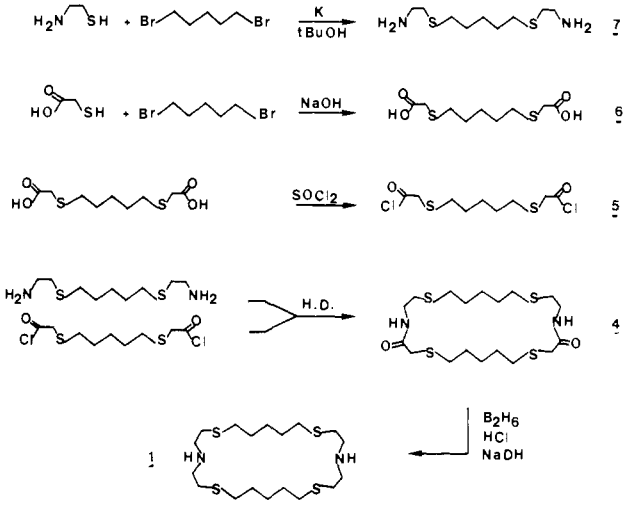

bridging ligands. The redox properties of the copper type 3 centers have been mimicked with some low molecular weight copper complexes that act as bielectronic donor–receptor systems.[1,12,13] The studies of binuclear copper(I) compounds and their reactivity toward carbon monoxide[14] or molecular oxygen are focused on model compounds for Cu(I)–protein interactions, especially reversible binding of oxygen and catalytic oxidation of organic substrates.[15,16]

The synthetic model approach to a binuclear type 3 active site has expanded the design of a number of binucleating ligands.[17]

Table I. Positional and Thermal (Supplementary Material) Parameters and Their Estimated Standard Deviations[a] for $[(CuCl_2)_2 \subset 1] \cdot 2H_2O$

	x	y	z
Cu(1)	0.9711 (1)	0.61559 (3)	0.59992 (5)
Cu(2)	0.0535 (1)	0.92809 (3)	0.69668 (5)
Cl(1)	0.8692 (2)	0.64260 (7)	0.7067 (1)
Cl(2)	0.9207 (4)	0.50819 (7)	0.6061 (1)
Cl(3)	0.1533 (2)	0.90617 (7)	0.57280 (8)
Cl(4)	0.9530 (2)	0.84064 (7)	0.7299 (1)
N(1)	0.0735 (6)	0.6064 (2)	0.5028 (2)
C(2)	0.987 (1)	0.6421 (2)	0.4361 (3)
C(3)	0.798 (1)	0.6380 (3)	0.4289 (4)
S(4)	0.7306 (2)	0.65769 (7)	0.5191 (1)
C(5)	0.7710 (8)	0..7374 (2)	0.5271 (3)
C(6)	0.6376 (9)	0.7727 (3)	0.4709 (4)
C(7)	0.678 (1)	0.8392 (3)	0.4708 (3)
C(8)	0.6753 (9)	0.8698 (3)	0.5473 (4)
C(9)	0.7211 (9)	0.9357 (2)	0.5450 (3)
S(10)	0.7663 (2)	0.96469 (7)	0.6442 (1)
C(11)	0.831 (1)	0.0406 (2)	0.6291 (4)
C(12)	0.019 (1)	0.0452 (2)	0.6271 (3)
N(13)	0.1187 (7)	0.0146 (2)	0.6953 (2)
C(14)	0.306 (1)	0.0209 (2)	0.6997 (4)
C(15)	0.3969 (9)	0.9932 (3)	0.7745 (4)
S(16)	0.3206 (2)	0.91829 (7)	0.7874 (1)
C(17)	0.4554 (9)	0.8748 (3)	0.7358 (4)
C(18)	0.411 (1)	0.8081 (5)	0.7468 (7)
C(19)	0.512 (1)	0.7681 (5)	0.7233 (9)
C(20)	0.461 (1)	0.7034 (4)	0.7257 (7)
C(21)	0.300 (1)	0.6899 (3)	0.6804 (5)
S(22)	0.2516 (2)	0.61138 (7)	0.6705 (1)
C(23)	0.3466 (9)	0.5876 (3)	0.5892 (4)
C(24)	0.2622 (9)	0.6170 (3)	0.5160 (4)
O(1)	0.1976 (7)	0.7770 (2)	0.5028 (3)
O(2)	0.032 (1)	0.7283 (2)	0.8446 (3)

[a] In parentheses.

Table II. Selected Bond Distances and Angles in the $[(CuCl_2)_2 \subset 1] \cdot 2H_2O$ Complex (in Å and deg) with Estimated Standard Deviations in Parentheses[a]

Cu(1)-Cl(1)	2.260 (1)	Cu(2)-Cl(4)	2.240 (1)
Cu(1)-Cl(2)	2.453 (1)	Cu(2)-Cl(3)	2.499 (1)
Cu(1)-N(1)	2.033 (5)	Cu(2)-N(13)	2.015 (4)
Cu(1)-S(4)	2.350 (1)	Cu(2)-S(10)	2.435 (1)
Cu(1)-S(22)	2.236 (1)	Cu(2)-S(16)	2.407 (1)
N(1)-Cu(1)-Cl(1)	170.1 (2)	N(13)-Cu(2)-Cl(4)	162.9 (2)
N(1)-Cu(1)-Cl(2)	91.9 (1)	N(13)-Cu(2)-Cl(3)	93.15 (9)
N(1)-Cu(1)-S(4)	86.8 (2)	N(13)-Cu(2)-S(10)	83.9 (2)
N(1)-Cu(1)-S(22)	86.9 (2)	N(13)-Cu(2)-S(16)	84.3 (2)
Cl(1)-Cu(1)-Cl(2)	98.07 (1)	Cl(4)-Cu(2)-Cl(3)	103.94 (1)
Cl(1)-Cu(1)-S(4)	90.79 (3)	Cl(4)-Cu(2)-S(10)	92.32 (3)
Cl(1)-Cu(1)-S(22)	91.57 (3)	Cl(4)-Cu(2)-S(16)	93.48 (3)
Cl(2)-Cu(1)-S(4)	107.61 (3)	Cl(3)-Cu(2)-S(10)	99.62 (3)
Cl(2)-Cu(1)-S(22)	94.80 (3)	Cl(3)-Cu(2)-S(16)	99.85 (3)
S(4)-Cu(1)-S(22)	156.90 (7)	S(10)-Cu(2)-S(16)	157.69 (7)

[a] Bond distances and angles in the macrocycle 1 are given in Table III available in supplementary material.

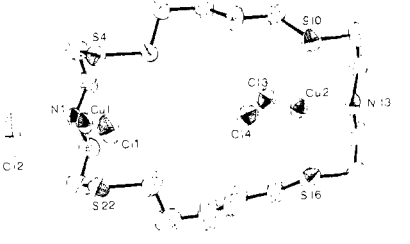

Figure 1. ORTEP view of 2 showing the boat-shaped structure of the macrocyclic ligand. Vibrational ellipsoids are drawn at the 50% probability level.

Here we report the synthesis of the binucleating macrocyclic ligand 1,13-diaza-4,10,16,22-tetrathiacyclotetracosane (**1**) and the studies

(9) (a) Haddad, M. S.; Hendrickson, D. N. *Inorg. Chim. Acta* **1978**, *28*, L121–L122. (b) Burk, P. L.; Osborn, J. A.; Youinou, M. T.; Agnus, Y.; Louis, R.; Weiss, R. *J. Am. Chem. Soc.* **1981**, *103*, 1273–1274. (c) Coughlin, P. K.; Lippard, S. J. *Ibid.* **1981**, *103*, 3228–3229. (d) McKee, V.; Dagdigian, J. V.; Ban, R.; Reed, C. A. *Ibid.* **1981**, *103*, 7000–7001.

(10) Davis, A. R.; Einstein, F. W. B.; Curtis, N. F.; Martin, J. W. L. *J. Am. Chem. Soc.* **1978**, *100*, 6258–6260. Churchill, M. R.; Davies, G.; El-Sayed, M. A.; El-Shazly, M. F.; Hutchinson, J. P.; Rupich, M. W.; Watkins, K. O. *Inorg. Chem.* **1979**, *18*, 2296–2300.

(11) Mc Fayden, W. D.; Robson, R. *J. Coord. Chem.* **1976**, *5*, 49–53. De Courcy, J. S.; Waters, T. N.; Curtis, N. F. *J. Chem. Soc., Chem. Commun.* **1977**, 572–573. Timmons, J. H.; Martin, J. W. L.; Martell, A. E.; Rudolf, P.; Clearfield, A.; Loeb, S. J.; Willis, C. J. *Inorg. Chem.* **1981**, *20*, 181–186. Mazurek, W.; Berry, K. J.; Murray, K. S.; O'Connor, M. J.; Snow, M. R.; Wedd, A. G. *Ibid.* **1982**, *21*, 3071–3080.

(12) (a) Gisselbrecht, J. P.; Gross, M.; Alberts, A. H.; Lehn, J. M. *Inorg. Chem.* **1980**, 1386–1388. (b) Gisselbrecht, J. P.; Gross, M. *Adv. Chem. Ser.* **1982**, *No. 201*, 109–137.

(13) Fenton, D. E.; Lintvedt, R. L. *J. Am. Chem. Soc.* **1978**, *100*, 6367–6375. Lintvedt, R. L.; Stecher-Kramer, L. *Inorg. Chem.* **1983**, *22*, 796–802.

(14) Pasquali, M.; Floriani, C.; Gaetani-Manfredotti, A. *Inorg. Chem.* **1980**, *19*, 1191–1197; **1981**, *20*, 3382–3383. Pasquali, M.; Marini, G.; Floriani, C.; Gaetani-Manfredotti, A.; Guastini, C. *Ibid.* **1980**, *19*, 2525–2531. Pasquali, M.; Floriani, C.; Gaetani-Manfredotti, A.; Guastini, C. *J. Am. Chem. Soc.* **1981**, *103*, 185–186. Kitagawa, S.; Munakata, M. *Inorg. Chem.* **1981**, *20*, 2261–2267. Gagne, R. R.; Kreh, R. P.; Dodge, J. A.; Marsh, R. E.; Mc Cool M. *Ibid.* **1982**, *21*, 254–261. Sorell, T. N.; Jameson, D. L. *J. Am. Chem. Soc.* **1982**, *104*, 2053–2054. Pasquali, M.; Floriani, C.; Ventini, G.; Gaetani-Manfredotti, A.; Chiesi-Villa, A. *Ibid.* **1982**, *104*, 4092–4099.

(15) Bulkowski, J. E.; Burk, P. L.; Ludmann, M. F.; Osborn, J. A. *J. Chem. Soc., Chem. Commun.* **1977**, 498–499. Simmons, M. G.; Wilson, L. J. *Ibid.* **1978**, 634–636. Korp, J. D.; Bernal, I.; Merill, C. L.; Wilson, L. J. *J. Chem. Soc. Dalton Trans.* **1981**, 1951–1956. Burnett, M. G.; Mc Kee, V.; Nelson, S. M.; Drew, M. G. B. *J. Chem. Soc., Chem. Commun.* **1980**, 829–831. Munakata, M.; Nishibayashi, S.; Sakamoto, H. *Ibid.* **1980**, 219–220. Karlin, K. D.; Dahlstrom, P. L.; Cozette, S. N.; Scensny, P. M.; Zubieta, J. *Ibid.* **1981**, 881–882. Karlin, K. D.; Gultneh, Y.; Hutchinson, J. P.; Zubieta, J. *J. Am. Chem. Soc.* **1982**, *104*, 5240–5242. Karlin, K. D.; Hayes, J. C.; Hutchinson, J. P.; Zubieta, J. *J. Chem. Soc., Chem. Commun.* **1983**, 376–378.

(16) Gagne, R. R.; Kreh, R. P.; Dodge, J. A. *J. Am. Chem. Soc.* **1979**, *101*, 6917–6927. Drew, M. G. B.; Mc Cann, M.; Nelson, S. M. *J. Chem. Soc., Dalton Trans.* **1981**, 1868–1878. Nelson, S. M.; Esho, F. S.; Drew, M. G. B. *J. Chem. Soc., Chem. Commun.* **1981**, 388–389. Hendriks, H. M. J.; Birker, P. J. M. W. L.; van Rijn, J.; Verschoor, G.C.; Reedijk, J. *J. Am. Chem. Soc.* **1982**, *104*, 3607–3617.

of two molecular bimetallic inclusion copper(II) complexes $[(CuCl_2)_2 \subset \mathbf{1}]$ (**2**) and $[Cu_2(N_3)_4 \subset \mathbf{1}]$ (**3**). The crystal and molecular structures, spectral and magnetic properties, and electrochemical behavior of **2** and **3** are presented and discussed in terms of potential models for copper–protein binuclear active sites.

The macrocycle **1** was designed to have two independent binding sites. The intermetallic distances resulting from the coordination of two metallic ions in **1** can be in the range 3.5–8 Å according to the flexibility relative to the five-membered linear carbon chains which are bridging the two binding sites. Taking into account the high positive standard potential occurring in the copper proteins, two SNS coordination sets in which the donor atoms are separated by two ethylene groups were chosen in regard of the best compromise between the enhanced stability of copper(I) with respect to copper(II) complexes. They are able to accommodate the different coordination geometries without major ligand conformational change during the redox processes.[18] Moreover, the binding sites do not saturate the copper coordination sphere, *both in the cupric and cuprous state*, in order to promote further complexation on the vacant metal positions and to test the transport properties or catalytic activity of such systems.

Results and Discussion

Synthesis of the Macrocyclic Ligand 1,13-Diaza-4,10,16,22-tetrathiacyclotetracosane, [24-ane-N_2S_4] (1), and of Its Bis Cu(II) Complexes 2 and 3. Ligand **1** was prepared by adapted literature procedures as outlined in Scheme I. It has been synthesized by high-dilution condensation[19a] of the required diamine **7** with the diacid chloride **5** to the corresponding cyclic bis-amide **4** followed by reduction with diborane in THF, hydrolysis with 6 N HCl at reflux, and treatment with aqueous sodium hydroxide.[19b] Ligand **1** forms complexes of 1:2 ligand–metal stoichiometry with copper(II) salts. **2** is obtained by addition of a stoichiometric amount of $CuCl_2$ to a solution of **1** in a mixture of methylbenzene–ethanol–methanol. In the same manner **3** is prepared by complexation of $Cu(NO_3)_2 \cdot 3H_2O$ with **1** followed by anion substitution by means of sodium azide.

Description of the Structure of $2 \cdot 2H_2O$. Positional and thermal parameters of the complex are given in Table I. Distances and angles of interest are presented in Tables II and III. The crystal structure of **2** consists of the packing of four discrete complex molecules of $[(CuCl_2)_2 \subset \mathbf{1}]$ and eight water molecules which afford intermolecular hydrogen binding in the unit cell. Figure 1 displays the complex molecule which possesses no crystallographic symmetry but adopts a pseudoplane of symmetry containing the two copper ions, the four chlorines, and the ligand's two nitrogens. The intermetallic separation in the molecule is 7.228 (1) Å. Each copper ion shows a square-based pyramidal environment formed by a NS_2Cl and Cl donor set. The copper ions Cu(1) and Cu(2) are displaced respectively by 0.46 (2) and 0.43 (2) Å out of the equatorial plane toward the axial chlorine. The bond lengths around the copper atoms in the square base are similar to those of covalent bonding of copper, taking into account the different nature of the ligating atoms. The Cu–N distances are 2.033 (5) and 2.015 (1) Å, the Cu–Cl are 2.260 (1) and 2.240 (1) Å, and the Cu–S lengths range from 2.236 (1) to 2.435 (1) Å.[20] The Cu–Cl axial distances of 2.453 (1) and 2.499 (1) Å are significantly greater than the Cu–Cl equatorial bonds, as expected.[21a] The macrocyclic ligand has a "boat" type conformation that brings the d_{z^2} copper orbitals pointing in two directions, approximatively perpendicular. The four chlorine atoms occupy positions that correspond to a stable conformation by minimizing the Cl···Cl interaction between the two inserted $CuCl_2$ units. The axial Cl(2) is pointed outside the macrocyclic covering whereas the other axial Cl(3) is located inside the macrocyclic cavity. This last position is favored by the proximity of the hydrophobic environment due to the five-membered carbon chains.

The crystalline cohesion is stabilized by the two water molecules O(1) and O(2) at 2.838 (8) Å apart. The packing in the unit cell is shown in Figure 2. In view of the nearest neighbor contacts

Table IV. Intermolecular Hydrogen Bonds and Intermetallic Distances (Å) in the Crystal Structure of $[(CuCl_2)_2 \subset 1] \cdot 2H_2O$ with their Estimated Standard Deviations in Parentheses

O(1)···O(2)	$4/01\bar{1}$[a]	2.839 (8)
O(1)···Cl(3)	1/000	3.197 (5)
O(2)···Cl(1)	1/000	3.168 (6)
O(2)···Cl(4)	1/000	3.214 (6)
N(1)···Cl(2)	2/211	3.214 (4)
N(13)···Cl(1)	$3/2\bar{1}1$	3.343 (4)
N(13)···Cl(2)	$3/2\bar{1}1$	3.559 (5)
Cu(1)···Cu(2)	1/000	7.228 (1)
Cu(1)···Cu(2)	$3/2\bar{1}1$	5.550 (1)
Cu(1)···Cu(1)	2/211	6.334 (1)
Cu(1)···Cu(2)	$4/01\bar{1}$	7.292 (1)
Cu(1)···Cu(1)	1/100	7.943 (1)

[a] The first symbol corresponds to the number of the symmetry-equivalent position: $1, x, y, z$; $2, \bar{x}, \bar{y}, \bar{z}$; $3, \bar{x}, y, \bar{z}$; $4, x, \bar{y}, z$. The second part of three numbers indicates the cell translations along each axis $(\vec{a}\ \vec{b}\ \vec{c})$. These indications are relative to the second atoms, the first one corresponding always to the 1/000 location.

Table V. Positional and Thermal (Supplementary Material) Parameters and Their Estimated Standard Deviations for $[Cu_2(N_3)_4 \subset 1]$

	x	y	z
Cu	0.52071 (5)	0.50000 (0)	0.77132 (5)
N(25)	0.3723 (3)	0.50000 (0)	0.8835 (3)
N(26)	0.3639 (3)	0.50000 (0)	0.9876 (3)
N(27)	0.3439 (3)	0.50000 (0)	0.0913 (3)
N(28)	0.3932 (4)	0.50000 (0)	0.6288 (3)
N(29)	0.2775 (4)	0.50000 (0)	0.6403 (3)
N(30)	0.1639 (5)	0.50000 (0)	0.6491 (4)
N(1)	0.6691 (3)	0.50000 (0)	0.6513 (3)
C(2)	0.7502 (3)	0.5921 (4)	0.6549 (3)
C(3)	0.6694 (4)	0.6832 (4)	0.6204 (3)
S(4)	0.5463 (1)	0.71577 (7)	0.72496 (8)
C(5)	0.6554 (4)	0.7822 (3)	0.8329 (4)
C(6)	0.5782 (4)	0.8430 (3)	0.9172 (4)
C(7)	0.50000 (0)	0.7790 (4)	0.00000 (0)

Table VI. Bond Distances (Å) for $[Cu_2(N_3)_4 \subset 1]$ with Their Estimated Standard Deviations in Parentheses

Cu(1)-N(1)	2.072 (3)	N(1)-C(2)	1.470 (5)
Cu(1)-N(25)	2.013 (3)	C(2)-C(3)	1.495 (7)
Cu(1)-N(27′)	1.994 (3)	C(3)-S(4)	1.810 (4)
Cu(1)-N(28)	1.987 (3)	S(4)-C(5)	1.812 (4)
Cu(1)-S(4)	2.919 (1)	C(5)-C(6)	1.494 (6)
		C(6)-C(7)	1.513 (5)
Cu(1)···Cu(2)[a]	5.145 (1)	N(25)-N(26)	1.170 (5)
Cu(1)···Cu(1′)[b]	6.043 (1)	N(26)-N(27)	1.187 (5)
		N(28)-N(29)	1.186 (6)
N(1)···N(28′)	3.149 (5)	N(29)-N(30)	1.160 (7)

[a] Intramolecular distance. [b] Intermolecular distance.

(17) Dickson, I. E.; Robson, R. *Inorg. Chem.* **1972**, *11*, 1777–1785. Lehn, J. M. *Pure Appl. Chem.* **1978**, *50*, 871–892 *Ibid.* **1980**, *52*, 2441–2459. Nelson, S. M. *Ibid.* **1980**, *52*, 2461–2476. Nelson, S. M. *Inorg. Chim. Acta* **1982**, *62*, 39–50. Fenton, D. E.; Casellato, U.; Vigato, P. A.; Vidali, M. *Ibid.* **1982**, *62*, 57–66. Martin, A. E.; Bulkowski, J. E. *J. Am. Chem. Soc.* **1982**, *104*, 1434–1436.

(18) Karlin, K. D.; Dahlstrom, P. L.; Stanford, M. L.; Zubieta, J. *J. Chem. Soc., Chem. Commun.* **1979**, 465–467. Karlin, K. D.; Dahlstrom, P. L.; Hyde, J. R.; Zubieta, J. *Ibid.*, **1980**, 906–908.

(19) (a) Stetter, H.; Mayer, K. H. *Chem. Ber.* **1961**, *94*, 1410–1416. Park, G. H.; Simmons, H. E. *J. Am. Chem. Soc.* **1968**, *90*, 2428–2431. Lehn, J. M.; *Struct. Bonding (Berlin)* **1973**, *16*, 1–69. (b) Brown, H. C.; Heim, P. *J. Org. Chem.* **1973**, *38*, 912–916.

(20) (a) Olmstead, M. M.; Musker, W. K.; Kessler, R. M. *Inorg. Chem.* **1981**, *20*, 151–157. (b) Ainscough, E. W.; Baker, E. N.; Brodie, A. M.; Larsen, N. G. *J. Chem. Soc., Dalton Trans.* **1981**, 2054–2058. (c) Dagdigian, J. V.; Mc Kee, V.; Reed, C. A. *Inorg. Chem.* **1982**, *21*, 1332–1342.

(21) (a) Marsh, W. E.; Hatfield, W. E.; Hodgson, D. J. *Inorg. Chem.* **1982**, *21*, 2679–2684. (b) Hamilton, W. C.; Ibers, J. A. "Hydrogen Bonding in Solids"; W. A. Benjamin: New York, **1968**. Emsley, J. *Chem. Soc. Rev.*, **1980**, *9*, 91–124.

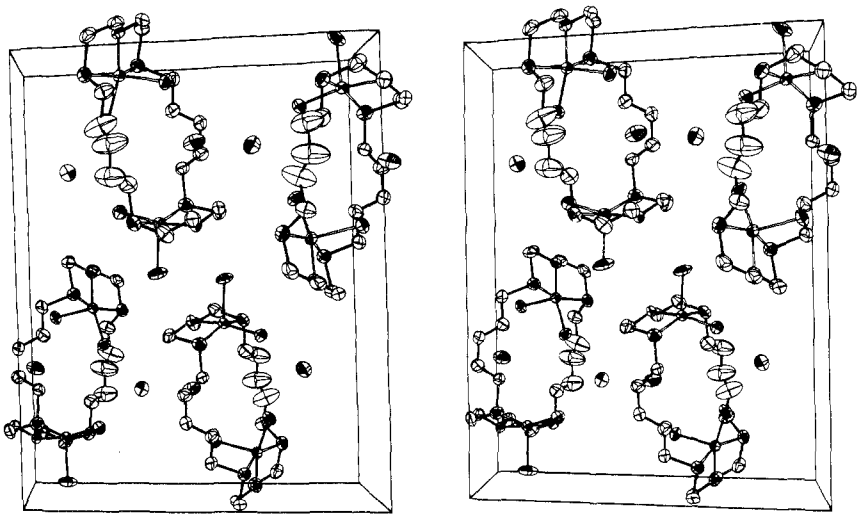

Figure 2. Stereodrawing of the packing in the unit cell for $2 \cdot 2H_2O$.

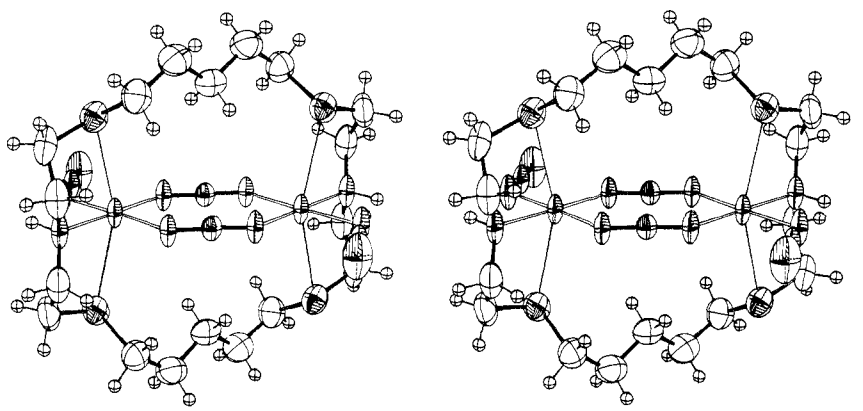

Figure 3. Stereodrawing of the molecular complex **3**.

Table VII. Angles (deg) for $[Cu_2(N_3)_4 \subset \mathbf{1}]$ with Their Estimated Standard Deviations in Parentheses

N(1)-Cu(1)-N(25)	178.2 (2)	N(25)-N(26)-N(27)	174.3 (4)
N(1)-Cu(1)-N(27′)	90.3 (1)	N(26)-N(27)-Cu(2)	126.8 (2)
N(1)-Cu(1)-N(28)	86.8 (1)	Cu(1)-N(28)-N(29)	120.7 (3)
N(1)-Cu(1)-S(4)	79.03 (7)	N(28)-N(29)-N(30)	178.6 (5)
N(25)-Cu(1)-N(27′)	91.6 (1)		
N(25)-Cu(1)-N(28)	91.4 (1)	N(1)-C(2)-C(3)	111.5 (4)
N(25)-Cu(1)-S(4)	100.83 (8)	C(2)-C(3)-S(4)	114.5 (3)
N(27′)-Cu(1)-N(28)	177.1 (2)	C(3)-S(4)-C(5)	97.4 (3)
N(27′)-Cu(1)-S(4)	94.12 (7)	S(4)-C(5)-C(6)	111.0 (3)
N(28)-Cu(1)-S(4)	85.33 (8)	C(5)-C(6)-C(7)	113.3 (3)
S(4)-Cu(1)-S(22)	156.58 (4)	C(6)-C(7)-C(8)	111.8 (3)
Cu(1)-N(25)-N(26)	136.0 (2)	C(24)-N(1)-C(2)	112.1 (4)

given in Table IV a hydrogen bonding network should occur between the N–H of the ligand, the water molecules, and the chlorine atoms.[21b] As a result of these hydrogen bonds, the intermolecular Cu···Cu separations become shorter than the intramolecular ones (see Table IV).

Description of the Structure of 3. The structure of **3** consists of discrete $[Cu_2(N_3)_4 \subset \mathbf{1}]$ molecules which present $2/m$ crystallographic symmetry (Figure 3). The positional and thermal parameters of the complex are given in Table V, bond distances and angles in Tables VI and VII. The copper(II) ions are located inside the macrocycle at 5.145 (1) Å apart and each linked to a $N(+S_2)$ ligand donor set, to one nitrogen of an end-on bound azide ion (N(28)–N(29)–N(30)), and to two nitrogens of two di-μ-1,3-azido end-to-end bridging azide ions (N(25)–N(26)–N(27)) giving a $Cu_2(N_3)_2$ eight-membered ring (Figure 4). The cyclic $Cu_2(N_3)_2$, the two end-on bound azide ions, and the two ligand nitrogen atoms lie in the crystallographic plane of symmetry. This fact implicates the two copper(II) environments as being strictly square based and coplanar. The equatorial plane is formed by

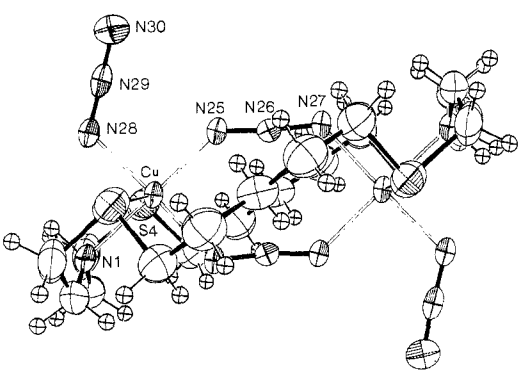

Figure 4. ORTEP view of **3** showing the chair-shaped structure of the macrocyclic ligand.

the four nitrogens N(1), N(25), N(27), and N(28); the Cu–N bond lengths are almost identical and range from 1.987 (3) to 2.072 (3) Å. The ligand sulfur atoms interact weakly with the d_{z^2} metallic orbitals since the observed Cu–S distance of 2.919 (1) Å is too long for covalent bonding.[22] The S–Cu–S bond angle is 156.58 (4)°. The observed S–Cu–S bond angles in copper complexes containing the diethylene–SNS chelating sequence range from 108.20 (7)°[18] in $[Cu^{II}(pam)SO_4]$ to 164.3 (3) in $[Cu_2(C_{24}H_{40}N_2O_2S_4)(NO_2)_2]^{2+}$.[9b] The angle of 108.20 (7)° corresponds to a cis location of the two sulfurs in a trigonal bipyramid. Angles in the range 121–122° have been observed

(22) Drew, M. G. B.; Cairns, C.; Nelson, S. M.; Nelson, J. *J. Chem. Soc., Dalton Trans.* **1981**, 942–948. Prochaska, H. J.; Schwindinger, W. F.; Schwartz, M.; Burk, M. J.; Bernarducci, E.; Lalancette, R. A.; Potenza, J. A.; Schugar, H. J. *J. Am. Chem. Soc.* **1981**, *103*, 3446–3455.

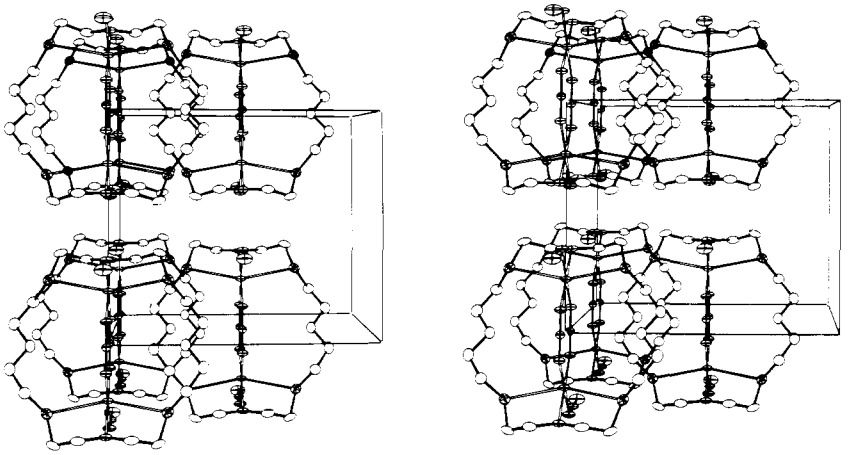

Figure 5. Stereodrawing of the packing in the unit cell for **3**.

in the corresponding tetrahedral copper(I) complexes. The most common positions are a trans location of the sulfur atoms in equatorial or axial positions of octahedral derived geometries with SCuS angles in the 155 to 165° range.[23] These features are significant of the versatility of this chelating unit for copper(II) and copper(I) especially if Cu(II) ↔ Cu(I) reversibility is required. The macrocycle adopts a chair shape. The ligand's nitrogen atoms are placed on both sides of the Cu–Cu axis (Figure 4). In spite of the shortened intermetallic distance in **3** with regard to the situation in **2** and the $2/m$ crystallographic symmetry carried by the ligand, no strain appears as shown by a survey of all bond distances and angles in the macrocycle. The two independent azide ions are almost linear, with N_α–N_β–N_γ bond angles of 174.3 (4)° for the bridging azido ligand and 178.6 (5)° for the end-on bound azide ion. The N_α–N_β and N_β–N_γ bond lengths are in the same range. In the end-on bound azide, a small difference in the two bond lengths can yet be noted, N_α–N_β 1.186 (6) Å and N_β–N_γ 1.160 (7) Å.[24]

Figure 5 shows the packing in the unit cell. Weak hydrogen bonding seems to take place between N(1) and N(28) belonging to adjacent molecules in view of N(1)···N(28′) distances of 3.149 (5) Å. This complex molecule association affords chains where the copper ions are nearly aligned along the direction of the $\vec{c}$ axis with alternatively 5.145 (1) Å (intramolecular) and 6.043 (1) Å (intermolecular) Cu···Cu separations. The planar $Cu_2(N_3)_2$ ring present in **3** is also encountered in the copper(I) compound $[Cu_2(PPh_3)_4(N_3)_2]$[25] and in the copper(II) complexes $[Cu_2(Me_5dien)_2(N_3)_2](BPh_4)_2$[26] and $[Cu_2(N_3)_4(C_{16}H_{38}N_6O_2)]$.[1c] The 24-membered macrocycle $C_{16}H_{38}N_6O_2$ containing two N_3 chelating units has been shown to yield in the presence of sodium azide a dinuclear Cu(II) complex that crystallizes in the same space group as **3** with all parameters almost identical. The same molecular stacking occurs and the intramolecular and intermolecular Cu···Cu distances are 5.973 and 5.980 Å, respectively.

Spectroscopy. Examination of IR spectra was useful in showing that the formation of the complex was effective. The frequencies for the ligand are similar in **2** and **3**. Several broad peaks between 3600 and 3400 cm^{-1} are indicative of hydrogen-bonding occurrence as expected from crystallographic investigations.[21b] Moreover, the two water molecules present in the crystalline state of **2** give a broad peak at 1610 cm^{-1}. The azido ligand present in **3** gives two stretching frequencies: a split sharp peak at 2065 and 2030 cm^{-1} and a weak peak at 1285 cm^{-1}, corresponding respectively to the asymmetric and the symmetric stretching frequencies.[27a]

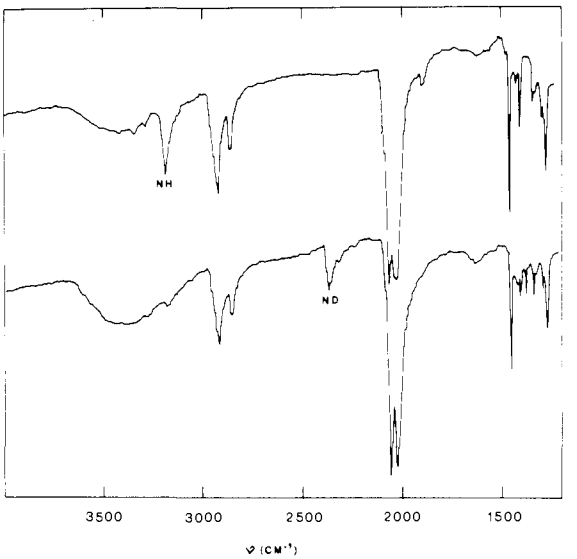

Figure 6. IR spectra of **3** and its deuterated derivative.

Table VIII. Absorption Maxima of the Binuclear Macrocyclic Complexes **2** and **3**

	λ_{max}, nm	ϵ, cm^{-1} M^{-1}	assignment
2[a]	710	650	d → d
			π_S → Cu(II)
	386	3700	σ_S → Cu(II)
			Cl(eq) → Cu(II)
	296	6200	Cl(apical) → Cu(II)
			lig. int. transition
3[a]	688	560	d → d
	404	4550	$\pi_{N_3^-}$ → Cu(II)
	296	4200	lig. int. transition

[a] Spectra were taken in Me_2SO solution.

Infrared spectroscopy also provides evidence for the presence of the proton on the nitrogen of the ligand. Indeed the diamagnetic behavior of **3** would also be consistent with the existence of two copper(III) cations complexed by a deprotonated ligand. Exchange of hydrogen with deuterium is obtained by synthesis of **3** in D_2O. Figure 6 shows the lack of the N–H stretching frequency and the presence of a N–D stretching frequency at 2350 cm^{-1}. This value agrees with the theoretical frequency of 2330 cm^{-1} obtained from

(23) Agnus, Y.; Louis, R. *Nouv. J. Chim.* **1981**, *5*, 305–309.
(24) N_α are the copper ligating nitrogens of the end-on bound azide ions. For a study of the electron density distribution in azide ions see: Stevens, E. D.; Hope, H. *Acta. Crystallogr., Sect A* **1977**, *A33*, 723–729.
(25) Ziolo, R. F. Gaugnan, A. P.; Dori, Z.; Pierpont, C. G.; Eisenberg, R. *Inorg. Chem.* **1971**, *10*, 1289–1296.
(26) Pierpont, C. G.; Hendrickson, D. N.; Daggan, D. M.; Wagner, F.; Barefield, E. K. *Inorg. Chem.* **1975**, *14*, 604–610.
(27) (a) Nakamoto, K.; in "Infrared spectra of Inorganic and Coordination Compounds"; Wiley, J., Ed.; Wiley-Interscience: New York, **1970**; 192. Addison, A. W.; Hendricks, H. M. J.; Reedijk, J.; Thompson, L. K. *Inorg. Chem.* **1981**, *20*, 103–110. (b) Colthup, N. B.; Daly, L. H.; Wiberley, S. E. "Introduction to Infrared and Raman Spectroscopy"; Academic Press: New York, **1964**; 168–190.

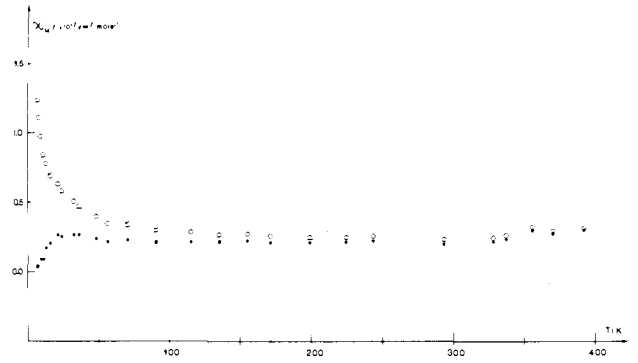

Figure 7. Magnetic susceptibility curve vs. temperature for **3**: experimental data (○) and χ_M corrected for the paramagnetic monomeric impurity (●).

the shift calculation of ν_{N-H} (3190 cm^{-1}) by deuterium exchange.[27b]

The electronic absorption spectra in solution of these complexes are given in Table VIII. In **2**, the presence of two sulfurs in trans positions in the copper coordination sphere induces a significant deformation of the square-based pyramid. This fact is responsible for the low-energy ligand-field band centered at 710 nm. The electronic spectra of copper thioether compounds are now well documented.[20,22] The thioether ligation to copper(II) leads to ligand-to-metal CT bands in the region of 300–600 nm according to the coordination geometry.[28,29] The broad maximum observed at 386 nm is attributed to a $\sigma_S \rightarrow$ Cu(II) charge-transfer transition. The intense high-energy band at 296 nm that occurs in **2** and **3** corresponds to charge-transfer transitions due to the ligand. The higher molecular extinction coefficient observed in **2** with regard to **3** can be attributed to the superposition in this region of Cl(apical) → Cu(II) ligand-to-metal CT bands. The equatorial chlorine also gives rise to ligand-to-metal CT bands in the region of 350 to 380 nm which are probably masked by the $\sigma_S \rightarrow$ Cu(II) ligand-to-metal CT band.[20b] In the same fashion, $\Pi_S \rightarrow$ Cu(II) ligand-to-metal CT can arise in the same region as the ligand-field transition, and probably the band at 710 nm is the envelope of two such bands since the molar absorptivity is quite high for d → d transitions only. It appears that the electronic spectrum of **2** confirms that it has the same conformation in solution as in the solid state. The electronic absorption spectrum of **3** presents three bands. The broad absorption at 688 nm corresponding to ligand-field transitions is significantly shifted to higher energies compared to that in **2**, according to the modification of the copper stereochemistry. The azido ligands give rise to intense $\Pi^*_{N_3^-} \rightarrow$ Cu(II) charge-transfer transitions at 404 nm. This CT transition energy is consistent with those observed for equatorial coordination of the azide ions to single Cu(II) centers.[2b,30] In some binuclear azide derivatives of hemocyanin and tyrosinase, besides the transition of normal tetragonal Cu(II)–N_3^- complexes at 400 nm, there are $\Pi_{N_3^-} \rightarrow$ Cu(II) CT transitions red-shifted to 500 nm corresponding to thinly-bound bridging azide ions.[2b,6,30] In fact, the strong covalent bonding for both end-on and end-to-end bound azides in **3** leads to similar CT-transition energies.

Magnetic Properties. Compound **2** follows Curie's law in the range 100–300 K with an effective magnetic moment of 1.79 μ_B/Cu^{2+}. This behavior, consistent with isolated uncoupled Cu(II) sites, agrees with the structural features, especially the large intermetallic distances and the lack of bridging ligands.

Variable-temperature magnetic susceptibility measurements were taken between 1.6 and 390 K. They show that the azide derivative **3** exhibits a diamagnetic behavior until a temperature of 382 K, where it explodes (Figure 7). The increase in χ_M at very low temperature is most likely due to a small amount of a monomeric paramagnetic impurity. Indeed, the variable temperature X-band EPR powder spectra of a weighted sample of **3** give rise to a signal with the following hamiltonian parameters: $g_\perp = 2.05$, $g_\parallel = 2.24$, $A_\parallel = 153$ G. The lack of the half-field, $\Delta M_s = 2$, transition is consistent with a monomeric copper(II) species. The integration of the EPR signals at several temperatures indicates that the compound follows Curie's law ($C = 0.013$ cm^3 K) and that about 1% of the copper present in the sample is responsible for the signal. We assigned the EPR signal to the presence of 1% of a paramagnetic impurity and we applied the corresponding correction to the experimental χ_M values. The resulting curve shows no variation of the magnetic susceptibility over the temperature range 1.6–390 K, indicating a very strong antiferromagnetic interaction between the copper ions in **3**.

Most of the known binuclear copper(II) complexes presenting large antiferromagnetic interaction have intermetallic distances in the range 3.2–3.7 Å. They are essentially monobridged compounds, with oxygen as bridging atom in the hydroxo form[9a–c] or belonging to a carbonato ligand[10] and dibridged binuclear species always with one hydroxo-like bridging ligand.[9d,11] A linear relation between the magnetic exchange parameter and the Cu–O–Cu bridging angle has been established in dibridged Cu(II) hydroxide complexes in the case of planar Cu_2O_2 cycles.[31] Since that time several structural features such as the distortion of the cyclic core,[32] the copper stereochemistry and its deformation, and the chemical function of the bridging oxygen[11] have been related to the magnitude of the antiferromagnetic coupling constant in this type of binuclear complex. The large exchange interaction mediated by the azide ligands in **3** has been explained by a semiquantitative molecular orbital analysis on a planar model with an idealized symmetry of D_{2h}. The orbital energies were obtained from extended-Hückel calculations, and according to the parameters used for the MO calculation, a singlet–triplet energy gap of 1.10 eV[1c] has been evaluated. This large energy is due to the predominant interaction between the ground state of the copper orbitals and the HOMO of the azide (nonbonding Π_g)[33] both of similar energies.

In the case of the complexes $[Cu_2(N_3)_4(C_{16}H_{38}N_6O_2)]$[1c] and $[Cu_2(N_3)_2(Me_5dien)_2](BPh_4)_2$,[26] the two magnetic orbitals have relative orientations particularly unfavorable for transmitting the electronic effects between the two Cu(II) ions through the bridging azide. The metallic spin densities are localized in parallel planes and the contribution of the d_{z^2} orbitals can give rise to an overlap with the bridging azides if the metallic ions are not too far away from each other. The small antiferromagnetic coupling observed in $[Cu_2(N_3)_2(Me_5dien)_2][BPh_4]_2$ should be explained by such an overlap. The paramagnetic behavior of $[Cu_2(N_3)_4(C_{16}H_{38}N_6O_2)]$ agrees with the lack of intermolecular interaction through hydrogen bonding; therefore the strong spin pairing in **3** is due only to intracavity interactions.

Thermodynamics and Electrochemistry. Determination of the protonation constants of **1** and the formation constant of the complexes with copper(II) perchlorate in methanol are under way.[34] The following results are obtained for the protonation constants of **1**: $\log K_1 = 9.74 \pm 0.04$ and $\log K_2 = 9.21 \pm 0.02$. The similar values for K_1 and K_2 can be attributed to the lack of electrostatic interactions between the protons of the two pro-

(28) Amundsen, A. R.; Whelan, J.; Bosnich, B. *J. Am. Chem. Soc.* **1977**, *99*, 6730–6739. Downes, M.; Whelan, J.; Bosnich, B. *Inorg. Chem.* **1981**, *20*, 1081–1086. Yamabe, T.; Hori, K.; Minato, T.; Fukui, K.; Sugiura, Y. *Ibid.* **1982**, *21*, 2040–2046.

(29) Miskowski, V. M.; Thich, J. A. Solomon, R.; Schugar, H. J. *J. Am. Chem. Soc.* **1976**, *98*, 8244–8350. Ainscough, E. W.; Brodie, A. M.; Palmer, K. C. *J. Chem. Soc., Dalton Trans.* **1976**, 2375–2381. Ainscough, E. W.; Baker, E. N. Brodie, A. M.; Larsen, N. G.; Brown, K. L. *Ibid.*, **1981**, 1746–1752.

(30) (a) Himmelwright, R. S.; Eickman, N. C.; Solomon, E. I. *J. Am. Chem. Soc.* **1979**, *101*, 1576–1586. Himmelwright, R. S.; Eickman, N. C.; Lubien, C. D.; Solomon, E. I. *Ibid.* **1980**, *102*, 5378–5388. (b) Beck, W.; Fehlhammer, W. P.; Pöllmann, P.; Schvierer, E.; Feldl, K. *Chem. Ber.* **1967**, *100*, 2335–2361.

(31) Hodgson, D. J. *Prog. Inorg. Chem.* **1975**, *19*, 173–241. Crawford, V. H.; Richardson, H. W.; Wasson, J. R.; Hodgson, D. J.; Hatfield, W. *Inorg. Chem.* **1976**, *15*, 2107–2110.

(32) Bencini, A.; Gatteschi, D. *Inorg. Chim. Acta* **1978**, *31*, 11–18. Charlot, M. F.; Jeannin, S.; Jeannin, J.; Kahn, O.; Lucrece-Abaul, J.; Martin-Frere, J. *Inorg. Chem.* **1979**, *18*, 1675–1681.

(33) Archibald, T. W.; Sabin, J. R. *J. Chem. Phys.* **1971**, *55*, 1821–1829.

(34) Arnaud-Neu, F.; Sanchez, M.; Schwing-Weill, M. J., to be published.

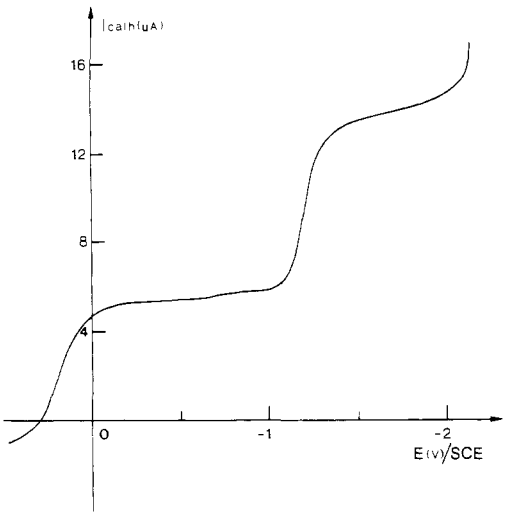

Figure 8. Two dielectronic reduction waves of **2**·2H_2O in Me_2SO and 0,1 M TEAP, on glassy carbon RDE (2000 rpm), (concentration of **2**·2H_2O = 2.9 × 10^{-4} M).

tonation sites which are far away from each other.[35] The formation constant β_{ijk} of the copper(II) complexes according to the equation

$$iM^{2+} + jH^{+} + kL \rightleftarrows (M_iH_jL_k)^{(2i+j)+}$$

(L = **1**) are log β_{101} = 9.84 ± 0.04 ($[CuL]^{2+}$), log β_{111} = 16.74 ± 0.06 ($[CuHL]^{3+}$), and log β_{201} = 12.9 ± 0.7 ($[Cu_2L]^{4+}$). The K constant corresponding to the formation of the binuclear cation $[Cu_2L]^{4+}$ from $[CuL]^{2+}$ and Cu^{2+} is log K = 3.04 ($K(\beta_{101}) = \beta_{201}$). These results show that the macrocyclic ligand **1** forms complexes of 1:1 and 1:2 stoichiometries but that the dissociation amount of the binuclear cation in solution, into the mononuclear species is very high. However, the complex formation or dissociation constant does not reflect the kinetic aspect of these reactions, and stable binuclear copper(II) complexes with **1** have been obtained by use of other stability factors such as the precipitation of the binuclear compound or the decrease of the whole charge of the complex by chelating anion coordination to $[Cu_2L]^{4+}$, leading to less charged cations, even neutral species, as is the case for **2** and **3**. As a consequence of these considerations, the yields in the synthesis of the binuclear compounds **2** and **3** are always small (10–20%).

The chloro derivative **2** gives, in a Me_2SO solution with 0.1 M tetraethylammonium perchlorate (TEAP), on a glassy carbon rotating disk electrode (RDE), two reduction waves at +0.20 V vs. SCE and −1.10 V vs. SCE.[1b] Each step is dielectronic as shown by the potentiostatic coulometry of each wave. (A platinum RDE gives rise to less well-defined signals, but the location of the half-wave potential is almost the same for the PtRDE as for glassy carbon RDE). The wave at +0.20 V vs. SCE is due to the reduction of the two Cu(II)s into two Cu(I)s which proceeds through two subsequent one-electron steps. The second wave at −1.10 V vs. SCE corresponds to the reduction of the bis Cu(I) compound into Cu(0) as confirmed by metallic copper deposit on the electrode (Figure 8). The log plot of the first Nernstian wave vs. potentials gives a slope of 142 mV/unit log[36] (slope = $\Delta E/\Delta \log (I/(I_d - I))$. No conclusion can be derived from this result since it corresponds to two successive monoelectronic steps from the bis Cu(II) to the bis Cu(I) species. However, the limiting cathodic currents are diffusion controlled, as indicated from the plot $1/I_{lim}$ vs. $1/\omega^{1/2}$ (linear through origin; ω, angular velocity). The cyclic voltammograms indicate that the first cathodic step Cu^{II}_2 to Cu^{I}_2 is quasi-reversible at low scan rates (<100 mV/s)

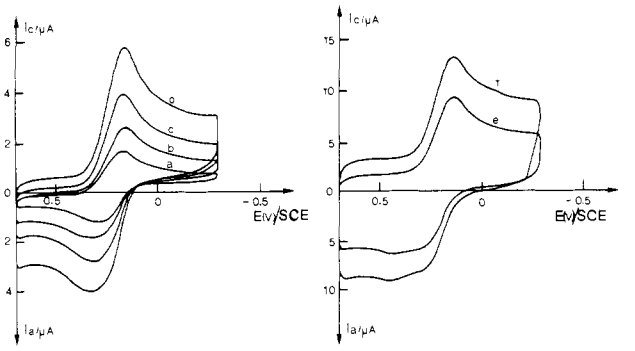

Figure 9. Cyclic voltammogram of the first reduction step ($2Cu^{II} \rightarrow 2Cu^{I}$) in **2**·2$H_2O$; c = 2.9 × 10^{-4} M; electrode: glassy carbon; solution: Me_2SO + 0.1 M TEAP; scan rates: (a) 10 mV s^{-1}, (b) 20 mV s^{-1}, (c) 50 mV s^{-1}, (d) 100 mV s^{-1}, (e) 200 mV s^{-1}, (f) 500 mV s^{-1}.

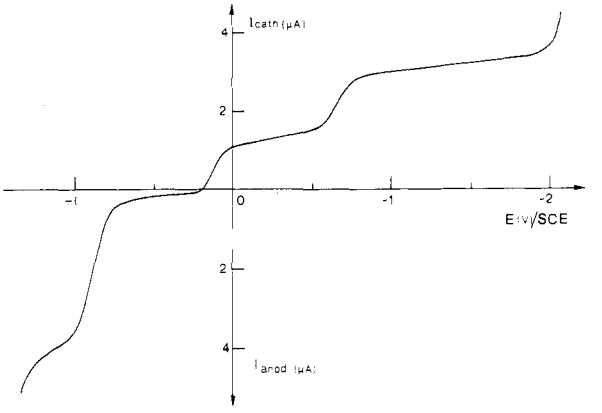

Figure 10. Two dielectronic reduction waves of **3**, in DMSO + 0.1 M TEAP on platinum RDE (2000 rpm), (c = 1.7 × 10^{-4} M).

Table IX. Cyclic Voltammetric Data for the Complexes **2** and **3**′ in Me_2SO

complexes	scan rate ν, V s^{-1}	E_{p_c}, mV	$E_{p_c/2}$, mV	E_{p_a}, mV	$E_{p_a/2}$, mV	ΔE_p, mV
2	0.010	170	270	295[a]	185	125
	0.020	170	270	300	190	130
	0.050	160	255	325	190	165
	0.10	165	260	320	190	155
	0.20	160	255	340	190	180
	0.50	140	235	-	190	-
	1.0	140	240	-	190	-
3	0.010	+24	100	120	40	96
	0.020	+20	96	124	42	104
	0.045	+15	94	128	44	113
	0.091	+20	98	130	46	110
	0.20	+12	94	132	48	120
	0.50	−10	90	139	55	149
	1.0	−37	80	163	70	200

[a] Data in this column correspond to the "less anodic" CV oxidation peak for **2**.

and results from the merging of two monoelectronic subsequent steps at $E_1°$ and $E_2°$ standard redox potentials, respectively.

$$[LCu^{II}_2] + e^- \overset{E_1°}{\rightleftarrows} [LCu^{II}Cu^{I}] + e^- \overset{E_2°}{\rightleftarrows} [LCu^{I}_2]$$

The difference between the formal potentials ($E_1°$ and $E_2°$), corresponding respectively to the first and the second electron transfer, was calculated according to the Myers and Shain method[37a] and is about 100 mV. For higher scan rates, the oxidation peak separates into two peaks corresponding to monoelectronic oxidation steps at significantly different potentials (>100 mV). This is due to the anodical shift of the second oxidation step. At

(35) Arnaud-Neu, F.; Schwing-Weill, M. J.; Louis, R.; Weiss, R. *Inorg. Chem.* **1979**, *11*, 2956–2961.
(36) Ammar, F.; Saveant, J. M. *J. Electroanal. Chem. Interfacial Electrochem.* **1973**, *47*, 215–221.
(37) (a) Myers, R. L.; Shain, I. *Anal. Chem.* **1969**, *41*, 980. (b) Polcyn, D. S.; Shain, I. *Ibid.* **1966**, *38*, 370–375. (c) Nicholson, R. S.; Shain, I. *Ibid.* **1964**, *36*, 706–723.

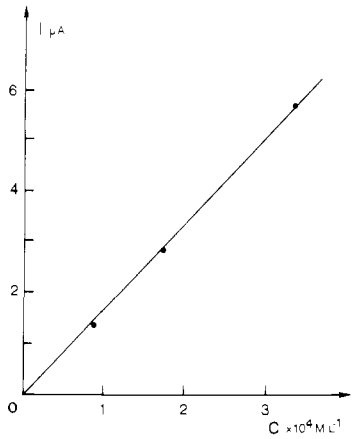

Figure 11. Standardization curve for oxidized azide titration obtained from the reduction wave at +0.88 V vs. SCE of NaN_3 in Me_2SO and 0.1 M TEAP on platinum RDE (2000 rpm).

the same time, the shape of the reduction peak remains unaffected for scan rates up to 500 mV/s (Figure 9). However, the parameter $E_{p_a}/2$ of the first oxidation step does not vary with the scan rate, indicative of a reversible process, whereas the second electron transfer corresponds to the rate-determining step (Table IX).

The electrochemical behavior of **3** was also investigated with the same techniques.[1b,12b] The voltammetry of **3** in Me_2SO on a platinum RDE shows three waves occurring at +0.88, +0.10, and −0.70 V vs. SCE (Figure 10). The signal at +0.88 V corresponds to the oxidation of azides. The study of the electrochemical behavior of sodium azide in Me_2SO by means of RDE polarograms was carried out for variable concentrations. The amplitudes of the signals localized at 0.88 V vs. SCE were used to draw a standardization curve (Figure 11). The correlation of the azide concentration in the complex solution with the standardization curve indicates that two out of four azide ions are oxidized. For concentrations of **3** lower than 10^{-4} M, the oxidized azide ratio rises to 2.6 azides per dimer. We have verified that for concentrations up to 10^{-4} M the ^1H NMR spectroscopy of **3** in Me_2SO-d_6 shows the compound to be diamagnetic. This result is consistent with the persistence of the doubly bridged core in the binuclear complex cation **3'** $[Cu_2(N_3)_2 \subset \mathbf{1}]^{2+}$ or possibly $[Cu_2(N_3)_2(Me_2SO)_2 \subset \mathbf{1}]^{2+}$ and the oxidation at 0.88 V of the two end-on bound azides which are released in solution after dissolution of **3**.

The second signal at +0.10 V corresponds to the dielectronic reduction from Cu(II)–Cu(II) to Cu(I)–Cu(I) in **3'**, as demonstrated by a reductive potentiostatic coulometry at 0.00 V involving two electrons, complete disappearance of the green color of the Me_2SO solution, and regeneration of the same color (identical electronic spectra) when the reduction is followed by coulometric oxidation at +0.30 V. The logarithmic analysis gives a slope of 90 mV/unit log leading to a difference of 72 ± 5 mV between the standard potentials $E_1°$ and $E_2°$, corresponding respectively to the first and the second monoelectronic reduction steps.[36] Besides, the linear plot of $1/I_{lim}$ vs. $1/\omega^{1/2}$ indicates that the reduction process is diffusion controlled without kinetic complication and is reversible. The last wave at −0.70 V is also dielectronic and corresponds to the reduction of Cu(I)–Cu(I) into metallic copper.

A cyclic voltammogram of **3'** at a platinum electrode is shown in Figure 12. The geometry of the peaks is in agreement with the value of $E_1° - E_2°$ already found.[37b] The peak potentials are independent of scan rate up to 0.1 V/s (Table IX). On the other hand, the Myers and Shain method[37a] leads to $E_1° - E_2° = 60 \pm 5$ mV. It follows that the standard potentials are $E_1° = +0.12$ V vs. SCE and $E_2° = +0.06$ V vs. SCE. Such a difference between the formal potentials indicates that the reduction of the first metallic site induces a stereochemical modification about the second metallic center which then becomes more difficult to reduce. Thus, the dinuclear species **3'** presents a behavior theo-

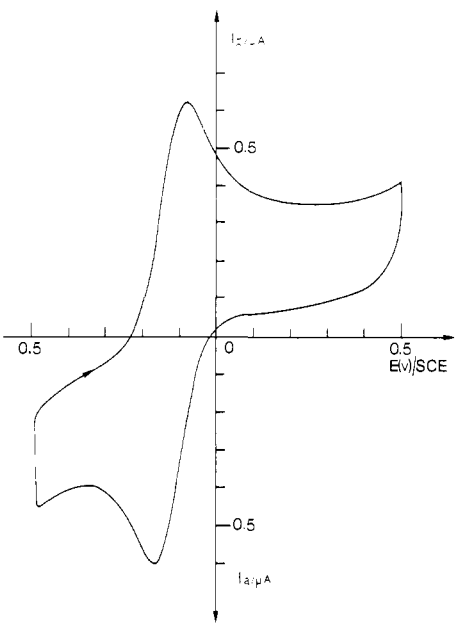

Figure 12. Cyclic voltammogram of the reduction step $Cu^{II}_2 \rightarrow Cu^{I}_2$ in **3**; $c = 3.5 \times 10^{-4}$ M: electrode: Pt; solution: Me_2SO and 0.1 M TEAP; scan rate: 10 mV s^{-1}.

Scheme II. Proposed Mechanism for the Reversible Redox Process of **3**: (a) Structure of **3** in the Solid State; (b) Possible Structure of the Cation $[Cu_2^{II}(N_3)_2 \subset \mathbf{1}]^{2+}$ in Me_2SO Solution; (c) Structure of the Molecule $[Cu_2^{I}(N_3)_2 \subset \mathbf{1}]$

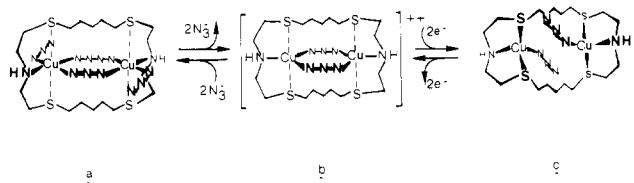

retically described by Shain[37c] corresponding to subsequent monoelectronic reduction with small difference between the standard potentials. In this case, cyclic voltammetry gives expanded peaks, the potential of which is independent of the scan rate.

The electrochemical results on dinuclear copper complexes[1b,12,13,39] have been related to the understanding of the physicochemical properties of the type **3** copper proteins that act as dielectronic acceptor–donor systems at high positive standard potentials.[3,38] Several structural features known to monitor the standard potential of the couple Cu(II)/Cu(I) have been underlined recently. The stabilization of the cuprous state relative to the cupric state corresponding to an anodical (or positive) shift of the redox potential is subjugated to sulfur coordination prior to oxygen and nitrogen, low symmetry of the copper stereochemistry, and environmental effects.[12,39-42] Compounds **2** and

(38) Malkin, R.; Malmström, B. G.; Vanngard, T. *Eur. J. Biochem.* **1969**, *10*, 324–329. Makino, N.; Ogura, Y. *J. Biochem. (Tokyo)* **1971**, *69*, 91–100. Reinhammar, B. R. M.; Vanngard, T. 1. *Eur. J. Biochem.* **1971**, *18*, 463–468. Reinhammar, B. R. M. *Biochim. Biophys. Acta* **1972**, *275*, 245–259. Makino, N.; Mc Mahill, P.; Mason, H. S.; Moss, T. H. *J. Biol. Chem.* **1974**, *249*, 6062–6066.

(39) Dockal, E. R.; Jones, T. E.; Sokol; W. F.; Engerer, R. J.; Rorabacher, D. B.; Ochrymowycz, L. A. *J. Am. Chem. Soc.* **1976**, *98*, 4322–4324. Gisselbrecht, J. P.; Gross, M.; *J. Electroanal. Chem. Interfacial Electrochem.* **1981**, *127*, 127–141. Anderson, O. P.; Perkins, C. M.; Brito, K. K. *Inorg. Chem.* **1983**, *22*, 1267–1273. Drago, R. S.; Desmond, M. J.; Corden, B. B.; Miller, K. A. *J. Am. Chem. Soc.* **1983**, *105*, 2287–2296.

(40) Yokoi, H.; Addison, A. W. *Inorg. Chem.* **1977**, *16*, 1341–1349. Addison, A. W.; Carpentier, M.; Lau, L. K. M.; Wicholas, M. *Ibid.* **1978**, *17*, 1545–1552.

(41) Patterson, G. S.; Holm, R. H. *Bioinorg. Chem.* **1975**, *4*, 257–275. James, B. R.; Williams, R. J. P. *J. Chem. Soc.* **1961**, 2007–2019. Addison, A. W.; Stenhouse, J. H. *Inorg. Chem.* **1978**, *17*, 2161–2165. Sorrel, T. N.; Jameson, D. L. *Ibid.* **1982**, *21*, 1014–1019. Fabbrizzi, L.; Lari, A.; Poggi, A.; Seghi, B. *Ibid.* **1982**, *21*, 2083–2085. Datta, D.; Chakravorty, A. *Ibid.* **1983**, *22*, 1085–1090.

Table X. Crystal Data and Number of Reflections for $[(CuCl_2)_2 \subset 1] \cdot 2H_2O$ (**2**) and for $[Cu_2(N_3)_4 \subset 1]$ (**3**)

	$[(CuCl_2)_2 \subset 1] \cdot 2H_2O$ (**2**·$2H_2O$)	$[Cu_2(N_3)_4 \subset 1]$ (**3**)
formula	$Cu_2C_{18}H_{42}N_2O_2S_4Cl_4$	$Cu_2C_{16}H_{36}N_{14}S_4$
M_r	715.68	705.93
space group	$P2_1/c$ (14)	$C2/m$ (12)
a, Å	7.943 (2)	10.126 (2)
b, Å	22.481 (6)	13.246 (3)
c, Å	17.538 (5)	11.156 (2)
β, deg	100.97 (2)	93.47 (1)
V, Å^3	3074.5	1493.6
Z, formula units	4	2
ρ_{obsd}, g cm^{-3}	1.56 (flotation in $CHCl_3$–CCl_4; 20 °C)	1.58 (flotation in $CHCl_3$–CCl_4; 20 °C)
ρ_{calcd}, g cm^{-3}	1.545	1.57
data collection temp, K	291	291
radiation, Å	graphite monochromated Cu, $\lambda(K\alpha) = 1.5418$	graphite monochromated Cu, $\lambda(K\alpha) = 1.5418$
linear coeff. abs, cm^{-1}	77	46
unique data	5050	1084
unique data with $F_o^2 > 3\sigma(F_o^2)$	3150	954
R_F, R_{wF}	0.048, 0.057	0.038, 0.051
estd stand devn of observn of unit wt	1.80	1.98

3 both undergo reversible reduction in an unique dielectronic step involving two monoelectronic transfers at almost identical, and positive, potentials. In the chloro derivative, the two Cu(II)s are structurally independent and the first reduction does not affect significantly the second Cu(II), which then is reduced at a nearly identical potential, the ligand NS_2 donor set around the copper being consistent with the positive redox potential. The analogous behavior exhibited by the highly symmetric compound **3**, where the copper centers are strongly linked by two end-to-end bridging azides, has been explained by the involvement of the sulfurs of the ligand during the electron transfers. Indeed, the ligand is able to accommodate a $[N + N_3]$ square planar stereochemistry for Cu(II), and a $[NS_2 + N]$ tetrahedral environment in the reduced state without large conformational change, owing to the flexibility of the five-membered carbon chain linking the two chelating units as pictured in Scheme II.

Experimental Section

Physical Measurements. Infrared spectra were taken as KBr pellets on a Perkin-Elmer 812 infrared spectrophotometer. Electronic absorption spectra were measured on a Cary 219 Model UV–vis spectrophotometer. Variable-temperature susceptibility measurements were recorded on a Foex–Forrer translation balance between 400 and 100 K and on a Foner magnetometer in the range of 4–120 K. The applied magnetic field was up to 0.7 T for **2** and up to 2.0 T for **3**. The independence of the susceptibility against the magnetic field was checked at several temperatures (293, 77, 4.2 K). $HgCo(SCN)_4$ and platinum metal were used for calibration. Diamagnetic corrections were applied for all non-metallic atoms using tabulated values of Pascal's constants. χ_D were estimated as -438×10^{-6} cm^3 mol^{-1} for **2** and -333×10^{-6} cm^3 mol^{-1} for **3**. The reproducibility of the magnetic curves of **3** was verified on different polycrystalline powder samples weighing in the range of 200-300 mg. X-band ESR spectra were recorded on a Bruker spectrophotometer using a Varian 10 kG magnet and equipped with a continuous-flow cryostat. Variable-temperature studies were accomplished on weighted powdered samples. Proton magnetic resonance spectra (NMR) were recorded on a Bruker Model 90 MHz. The chemical shifts are expressed in δ values (ppm) relative to tetramethylsilane as internal standard (s, singlet; t, triplet; m, multiplet). Elemental analyses were performed by the service Central d'Analyses du C.N.R.S. de Strasbourg.

The electrochemical measurements were carried out at 25 °C on platinum or glassy carbon electrodes used as rotating disk electrodes (RDE), rotating at 250 to 5000 rpm. Experiments were performed in dimethyl sulfoxide (Me_2SO distilled over CaH_2 prior to use) containing tetraethylammonium perchlorate (TEAP, recrystallized twice in methanol and dried at 60 °C under vacuum 48 h before use). Throughout the measurements, the reference electrode was a calomel electrode in a saturated aqueous solution of KCl (SCE) electrically connected with the studied solution by a junction bridge filled with the solvent and the background electrolyte used in the cell. The measurements were performed with an electrochemical device, Taccussel Model SOLEA, comprising a potentiostat, a voltage pilot unit, a current potential converter, and a potentiometric XY recorder (IFELEC IF 3802). The same device was used for cyclic voltammetric measurements at scan rates up to 1 V s^{-1}; for higher scan rates, the signal was stored in a two-channel transient recorder (BRYANS 512 A) before restitution with delay, on the potentiostatic XY recorder. Potentiostatic coulometry provided the amount of Faradays exchanged per mole of macrocyclic compound.

Crystal Structure Determination. X-ray Study of $[(CuCl_2)_2 \subset 1] \cdot 2H_2O$ (2·2H$_2$O). Well-formed crystals of **2**·$2H_2O$ were obtained from an aqueous ethanol–benzene solution left standing at room temperature. Precise lattice constants and diffracted intensities were derived from measurements carried out on a Philips PW 1100 diffractometer. The setting angles of 25 reflections with high 2θ values were determined by using the automatic centering program supplied with the computer-controlled diffractometer. Least-squares refinement of these reflections led to the lattice constants reported in Table X. Intensity data were collected by θ–2θ scanning using graphite monochromated Cu Kα radiation at a scan rate of 1.92° min^{-1}. The intensities were measured out to a $(\sin\theta)/\lambda$ of 0.53 Å^{-1} and the scan range employed was $1.25 \pm 0.28 \tan\theta$. At both ends of the peaks, the background was measured during half-time of the scanning time. The intensities of three standard reflections were monitored throughout the data collection and measured every 90 min. A total of 5050 independent intensities were collected and used for structure determination by direct methods; 3050 data having $I \geq 3\sigma I$ were retained for the refinement of the structure. The intensity data were reduced to a set of relative-squared amplitudes $|F_o|^2$ by application of the standard Lorentz and polarization factors. No absorption correction was applied.

Solution and Refinement of the Structure of 2·2H$_2$O. The structure was solved by direct methods. The coordinates of the two copper, the four sulfur, and the four chlorine atoms were obtained from a Karle–Fourier synthesis derived from the best nontrivial MULTAN solution. When the calculated contribution of these atoms was used to determine the phases, a Fourier synthesis revealed all non-hydrogen atoms defining the complex. In all structure-factor calculations, the atomic scattering factors used were taken from the usual sources.[43] The effect of anomalous dispersion was included for copper, sulfur, chlorine, and oxygen atoms. The values of $\Delta f'$ and $\Delta f''$ used are those given in ref 44. The structure was refined by full-matrix least-squares methods. The quantity minimized was $\sum w(|F_o| - |F_c|)^2$, where the weights w were taken as $1/\sigma(F_o)^2$. All non-hydrogen atoms were refined assuming anisotropic thermal motion. The contribution of hydrogen was introduced in calculated positions (C–H = 1.00 Å). These hydrogens were assumed to have isotropic thermal motion equal to 4.0. The final values of $R_F = \sum||F_o| - |F_c||/\sum|F_o|$ and $R_{wF} = |\sum w|F_o| - |F_c||^2/\sum w|F_o|^2|^{1/2}$ are given in Table X. The final atomic positional and thermal parameters are listed in Table I.

X-ray Study of $[Cu_2(N_3)_4 \subset 1]$ (3). Approximately cubic crystals of **3**, suitable for an X-ray study although they did exceed 100 μm of edge, were obtained by slow precipitation of the complex from an aqueous

(42) Addison, A. W.; *Inorg. Nucl. Chem. Lett.* **1976**, *12*, 899–903. Gagne, R. R.; Koval, C. A.; Smith, T. J. *J. Am. Chem. Soc.* **1979**, *101*, 4571–4580. Gagne, R. R.; Spiro, C. L.; Smith, T. J.; Hamann, C. A.; Thies, W. R.; Shiemke, A. K. *Ibid.* **1981**, *103*, 4073–4081. Long, R. C.; Hendrickson, D. N.; **1983**, *105*, 1513–1521.

(43) Vand, V.; Eiland, F. P.; Pepinsky, R. *Acta Crystallogr.* **1957**, *10*, 303–306. Forsyth, J. B.; Wells, M. *Ibid.* **1959**, *12*, 412–415. Moore, F. H. *Ibid.* **1963**, *16*, 1169–1175.

(44) Cromer, D. T. *Acta Crystallogr.* **1965**, *18*, 17–23.

ethanol solution with 10% Me_2SO (or DMF or propylene carbonate (PC)) [Cu(II)] $\sim 2 \times 10^{-5}$ M). The lattice parameters and the data collection were obtained as described for compound **2**·$2H_2O$, aside from the scan rate, which was 2.4° min^{-1} for **3**. Crystal data and details of the data collection are summarized in Table X. The structure was solved by the heavy-atom method. The coordinates of the independent copper atom were obtained from a three-dimensional Patterson function; the complete solution and refinement of the structure were carried out in the same way as that of **2**·$2H_2O$. The final atomic positional and thermal parameters are listed in Table V.

Synthesis of Compounds. All chemicals were reagent grade and utilized without further purification.

1,11-Diamino-3,9-dithiaundecane (1,5-Bis((β-aminoethyl)thio)pentane, 7). In a 2-L three-necked flask equipped with a reflux condenser and a dropping funnel, 1 L of *tert*-butyl alcohol and 47.0 g (1.2 mol) of potassium were mixed. After complete formation of the potassium *tert*-butylate, 68.2 g (0.6 mol) of cysteamine chlorohydrate was added. The heterogeneous mixture was refluxed for 30 min, and then 69.0 g (0.3 mol) of 1,5-dibromopentane was slowly added. The reflux was maintained 3 h. After cooling, the mixture was filtered and the filtrate reduced by vacuum evaporation. The residue was twice chromatographed over neutral alumine with methylbenzene as eluant. The solution was evaporated to dryness under vacuum to give a light yellow oil which solidified upon standing at room temperature (yield 80%). Anal. Calcd for $C_9H_{20}N_2S_2$: C, 49.05; H, 9.15; N, 12.71. Found: C, 49.81; H, 9.98; N, 12.01. ^1H NMR (C_6D_6/Me_4Si): δ 1.08 (s, 4 H, H_2NCH_2–), 1.37 (m, 6 H, $-SCH_2(CH_2)_3CH_2S$–), 2.28 (t, 4 H, $SCH_2(CH_2)_3$–), 2.33–2.63 (m A_2B_2, 8 H, $NH_2CH_2CH_2S$–).

3,9-Dithiaundecanedicarboxylic Acid (6). In a three-necked flask equipped with a reflux condenser and a dropping funnel 32.4 mL (0.5 mol) of mercaptoacetic acid was solubilized in 50 mL of water and 50 mL of ethanol. A solution of 40 g (1 mol) of sodium hydroxide in 50 mL of water was added. The solution was warmed to reflux and 24 g (0.25 mol) of dibromopentane was added dropwise. At the end of the addition, reflux was maintained 2 h. The resulting solution was evaporated to dryness under vacuum and the white residue was treated with 300 mL of 6 N HCl. The diacid was then extracted with diethyl ether. The collected organic phases were dried over sodium sulfate, filtered, and reduced by vacuum evaporation until precipitation began. After cooling at −30 °C, the white precipitate was filtered and washed with methylbenzene. The crude product can be recrystallized from boiling methylbenzene: mp 96 °C; yield 85%. Anal. Calcd for $C_9H_{16}O_4S_2$: C, 42.84; H, 6.39. Found: C, 41.89; H, 5.98; N, 0.0. ^1H NMR ($CDCl_3/Me_4Si$) δ 1.52 (m, 6 H, $SCH_2(CH_2)_3CH_2S$), 2.55 (t, 4H, SCH_2CH_2), 3.18 (s, 4 H, SCH_2COOH), 11.18 (s, 2 H, COOH).

3,9-Dithiaundecanedicarboxylic Acid Chloride (5). In a 500-mL flask equipped with a reflux condenser 25.23 g (0,1 mol) of **6**, 100 mL of benzene, and an excess of pure thionyl chloride or oxalyl chloride were mixed. The mixture was stirred at room temperature and in the darkness until all the diacid had reacted (approximately 24 h). The resulting solution was reduced to dryness under vacuum without the temperature exceeding 30 °C. The acid chloride was purified by precipitation in pentane at −80 °C. The light yellow oil was stored at −30 °C (yield 90%); ^1H NMR ($CDCl_3/Me_4Si$) δ 1.48 (m, 6 H, $SCH_2(CH_2)_3CH_2S$), 2.61 (t, 4 H, SCH_2CH_2), 3.20 (s, 4 H, SCH_2 COCl).

1,13-Diaza-4,10,16,22-tetrathia-2,12-dioxocyclotetracosane (4). A 0.100 M methylbenzene solution (1000 mL) of **7** and 1000 mL of a 0.050 M methylbenzene solution of **5** were placed in the two dropping funnels, on the high dilution setting, of a large flask equipped with a mechanical stirrer and containing 2 L of methylbenzene. The high dilution condensation was carried out under an inert atmosphere. At the end of the dropwise addition (1.5 mL min^{-1}) of the two reactants, the mixture was filtered to eliminate the formed dichlorhydrate of **7**. The filtrate was evaporated to dryness. The white residue was recrystallized from hot methylbenzene: Yield 60%; mp 116 °C. Anal. Calcd for $C_{18}H_{34}O_2N_2S_4$: C, 49.29; H, 7.82; N, 6.39. Found: C, 48.94; H, 7.31; N, 6.33. ^1H NMR ($C_6D_5CD_3/Me_4Si$) δ 1.51 (m, 12 H, SCH_2 $(CH_2)_3CH_2S$), 2.40–2.50 (m, 12 H, $-CH_2SCH_2(CH_2)_3CH_2S$ CH_2–), 3.07 (s, 4 H, $HNCOCH_2S$), 3.35–3.38 (q, 4 H, $HNCH_2CH_2S$), 6.83 (m, 2 H, NH).

1,13-Diaza-4,10,16,22-tetrathiacyclotetracosane (1). The cyclic bisamide **4** was reduced with diborane in THF. In a cooled 1-L two-necked flask flushed by argon 6.3 g (0.014 mol) of **4** in 150 mL of THF was mixed. By means of a syringe, 30 mL of a 1.1 M B_2H_6 solution was added slowly to the cooled solution. The mixture was then refluxed for 2 h. After cooling, the excess diborane was destroyed with a few milliliters of water. The mixture was evaporated to dryness, treated with 40 mL of 6 N HCl, and refluxed for 4 h. The mixture was reduced by vacuum evaporation and the residue treated with aqueous tetraethylammonium hydroxide. The cyclic diamine **1** was extracted with ether and chloroform. The organic phases were dried over sodium sulfate, filtered, and vacuum evaporated. The best purification method uses the conversion of **1** to its bis(chlorohydrate). The crude diamine **1** was treated with an aqueous ethanolic 3 N HCl solution until an homogeneous solution was obtained. After vacuum filtering, the solution was treated with a concentrated sodium hydroxide solution to pH 7–8; the diamine precipitated in fine needles. After cooling, the diamine was separated from the solution by vacuum filtering, dried under vacuum, and stored under argon. The white diamine fuses at approximately 35 °C (yield 80%). Anal. Calcd for $C_{18}H_{38}N_2S_4$: C, 52.63; H, 9.32; N, 6.82; Found: C, 52.93; H, 9.51; N, 6.82. ^1H NMR ($C_6D_5CD_3$, Me_4Si) δ 1.45 (m, 12 H, $SCH_2(CH_2)_3CH_2S$), 2.07 (m, 2 H, NH), 2.34 (t, 8 H, $SCH_2(CH_2)_3$), 2.45–2.64 (m, A_2B_2, 16 H, $HN(CH_2)_2S$).

[(CuCl$_2$)$_2$⊂1]·2H$_2$O: 2·2H$_2$O. The copper(II) complex with chloride was prepared by mixing an aqueous methanolic solution of $CuCl_2 \cdot H_2O$ (2×10^{-4} mol) and a solution containing 10^{-4} mol of the ligand **1** dissolved in a minimum of methylbenzene or benzene and diluted with ethanol. The resulting solution was filtered and slow evaporation of the filtrate gave dark-green crystals which were collected by filtration. Anal. Calcd for $C_{18}H_{42}Cu_2Cl_4N_2O_2S_4$: C, 30.21; H, 5.91; N, 3.91. Found: C, 30.09; H, 5.85; N, 3.85.

[Cu$_2$(N$_3$)$_4$⊂1] (3). The copper(II) complex with azide was prepared in the same manner as **2** by using $Cu(NO_3)_2 \cdot 3H_2O$ (2×10^{-4} mol) and sodium azide (4×10^{-4} mol) in aqueous solution. This preparation gave a crude product which precipitates rapidly as a fine brown powder of poor purity. Recrystallization in solvents such as Me_2SO, DMF, or propylene carbonate, where the material is soluble, was followed by the dissociation of **3** into a mononuclear complex. The best method to obtain a pure compound for physical measurements and structure determination was to retard the initial precipitation by diluting the mother liquor containing a 1/2 ratio of ligand–$Cu(NO_3)_2 \cdot 3H_2O$ to 100 mL with 10 mL of Me_2SO and a 50/50 aqueous ethanol solution. After that the aqueous sodium azide solution was added, and a brown-yellow solution was obtained in which the crystalline binuclear complex deposits overnight in cubes of approximately 100 μm edge. The product was filtered and washed with water. Anal. Calcd for $C_{18}H_{38}Cu_2N_{14}S_4$: C, 30.63; H, 5.43; N, 27.78. Found: C, 30.98; H, 5.52; N, 26.67. The compound explodes near 110 °C.

Acknowledgment. We thank M. Sanchez, Dr. F. Arnaud-Neu, and Professor M.J. Schwing-Weill for the provision of results prior to publication.

Supplementary Material Available: Tables I and V (positional and thermal parameters) and structure factors for **2**·$2H_2O$ and **3**, and Table III showing bond distances and angles in the macrocycle **1** in the crystalline structure of **2**·$2H_2O$ (16 pages). Ordering information is given on any current masthead page.